

Ligand solid-solution tuning of magnetic and mechanical properties of the van der Waals metal-organic magnet $\text{NiCl}_2(\text{btd})_{1-x}(\text{bod})_x$

Emily Myatt,¹ Simrun Lata,¹ Jem Pitcairn,¹ Dominik Daisenberger,² Silva M. Kronawitter,³ Sebastian A. Hallweger,³ Gregor Kieslich,³ Stephen P. Argent,¹ Jeremiah P. Tidey,⁴ Matthew J. Cliffe,^{*1}

Received Date
Accepted Date

DOI: 00.0000/xxxxxxxxxx

Van der Waals (vdW) magnets offer unique opportunities for exploring magnetism in the 2D limit. Metal-organic magnets (MOM) are of particular interest because functionalising the organic ligands allows for control over their physical properties. Here, we demonstrate tuning of mechanical and magnetic functionality of a recently reported non-collinear vdW ferromagnet, $\text{NiCl}_2(\text{btd})$ (btd = 2,1,3-benzothiadiazole), through creating solid-solutions with the oxygen-substituted analogue ligand 2,1,3-benzoxadiazole (bod). We synthesise solid-solutions, $\text{NiCl}_2(\text{btd})_{1-x}(\text{bod})_x$, up to $x = 0.33$ above which we find mixtures form, primarily composed of a new 1D coordination polymer $\text{NiCl}_2(\text{bod})_2$. Magnetometry on this series shows that bod incorporation reduces the coercivity significantly (up to 60%), without significantly altering the ordering temperatures. Our high pressure synchrotron diffraction measurements up to 0.4 GPa demonstrate that the stiffest axis is the *b* axis, through the Ni-N-(O/S)-N-Ni bonds, and the softest is the interlayer direction. Doping with bod fine-tunes this compressibility, softening the

layers, but stiffening the interlayer axis. This demonstrates how mixed-ligand strategy can be used to realise targeted magnetic and mechanical properties in vdW MOMs.

The modularity of metal-organic materials means that compounds with identical structural topologies but different ligands can be readily synthesised (they are ‘isoreticular’).¹ This in turn enables the synthesis of diverse and extensive ligand solid-solutions,^{2,3} which allows control of chemical function, e.g. methane separation⁴ and catalytic activity⁵. The physical properties of metal-organic frameworks (MOFs), e.g. mechanical,⁶ magnetic,⁷ or electronic⁸ function, can equally be controlled through ligand solution. There remains a great deal to learn about the physical properties of mixed-ligand MOFs, especially the possibility of creating function that goes beyond the linear combination of stoichiometric end-members.⁹ Recent work has shown that ligand solid-solutions in zeolitic imidazolate frameworks (ZIFs) subtly modulate the magnetic ordering temperatures of *rod* topology ZIFs¹⁰ and control the pressure-induced pore closing ZIF-4 analogues,^{11,12} and that solid-solutions of terminal halide ligands in $\text{Cr}(\text{pyz})_2\text{Br}_x\text{I}_{2-x}$ produce temperature-induced valence tautomeric transitions not present in the stoichiometric phases.¹³

Ligand solid-solution control over mechanical and magnetic function in vdW magnets is of special interest because pressure- and strain-control over magnetic function can be readily achieved in devices.¹⁴ This is particularly true for noncollinear magnets, where continuous evolution of magnetic order and properties is possible.¹⁵ We have recently reported a family of new layered MOMs with non-collinear magnetic structures, including the canted ferromagnet $\text{NiCl}_2(\text{btd})$.¹⁶ This material consists of NiCl_2 chains coordinated by the nitrogens of the nonlinear btd ligand to form corrugated sheets [Fig. 1]. The easy-axis ferromagnetic

¹ School of Chemistry, University of Nottingham, University Park, Nottingham, NG7 2RD, United Kingdom Email: matthew.cliffe@nottingham.ac.uk

² Diamond Light Source, Chilton, Didcot OX11 0DE, United Kingdom

³ TUM Natural School of Sciences, Technical University of Munich, D-85748 Garching, Germany

⁴ Department of Physics, University of Warwick, Gibbet Hill Road, Coventry, CV4 7AL, United Kingdom

† Electronic Supplementary Information (ESI) available: Additional experimental details, laboratory X-ray data, high pressure X-ray diffraction data, magnetic data, single crystal-derived structural models of $\text{NiCl}_2(\text{bod})$, $\text{NiCl}_2(\text{btd})$ and $\text{NiCl}_2(\text{bod})_2$ (PDF, CIF). Data for this article, including diffraction and magnetic data, with analysis scripts available at doi:10.17639/nott.7454. Crystallographic data has been deposited at the CCDC with reference numbers 2373766, 2373767 and 2377919 and can be obtained from <https://www.ccdc.cam.ac.uk/structures/>. See DOI: 10.1039/b000000x/

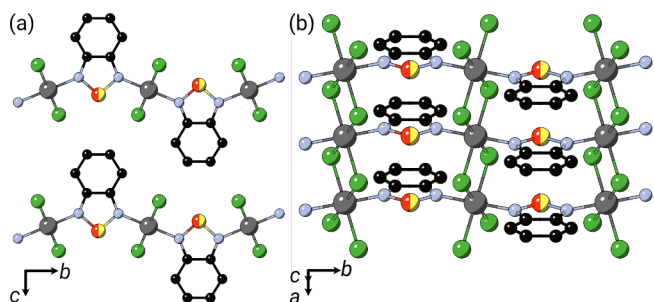


Fig. 1 Structure of $\text{NiCl}_2(\text{btd})_{1-x}(\text{bod})_x$ (a) viewed along the [100] direction (b) viewed along the [101] direction. C = black; Ni = grey; Cl = green; N = blue; O/S = red/yellow and H atoms omitted for clarity.

chains in combination with the tilting of chains induced by the ligand geometry, leads to noncollinear canted ferromagnetism with significant coercive field, $\mu_0 H_c = 1.0(1)$ T. The modularity of this system, together with the promise of its magnetic function, prompted us to investigate how substitution of the btd ligand for bod will affect both the structure, and the magnetic and mechanical properties of this MOM.

Our previous work established that $\text{NiCl}_2(\text{btd})$ can be made phase pure and crystalline through the direct reaction of $\text{NiCl}_2 \cdot 6\text{H}_2\text{O}$ and btd,¹⁶ and thus we first explored this approach to create the solid-solutions $\text{NiCl}_2(\text{btd})_{1-x}(\text{bod})_x$, attempting syntheses with target bod fraction, $x_t = 0, 0.25, 0.5, 0.75$ and 1.0 [ESI Section S1].

Analysis of the powder X-ray diffraction (PXRD) data confirmed that we were able to produce the desired phase up to $x_t \leq 0.75$ [Fig. 2 ESI Fig. S2], however, we found that the pure bod phase did not form. Consequently, we synthesised a series through the reaction of ethanolic solutions of nickel chloride and ligands over the same target range of x_t , analogous to $\text{CoCl}_2(\text{btd})$.¹⁷ We found by analysis of PXRD data that this again produced powders isostructural to $\text{NiCl}_2(\text{btd})$ up to $x_t \leq 0.75$, but at $x_t = 1$ we obtained a phase mixture for which primary phase was unknown. The purity of all other compounds was assessed using Pawley refinement of the PXRD data, which showed that the samples synthesised through direct reaction contained very small quantities of starting material, but that the solution-synthesised samples had broader diffraction peaks, likely due to small particle sizes [Fig. 2 (b), ESI Section S2.1].

The phase mixture formed during solution synthesis with $x_t = 1$ included a number of small single crystals (further details of the single crystal diffraction characterisation can be found in the ESI Sections S2.3, S2.4). We isolated a larger crystal ($63 \times 14 \times 10 \mu\text{m}^3$) which we found using single crystal X-ray diffraction to be a new 1D coordination polymer $\text{NiCl}_2(\text{bod})_2$, containing octahedrally coordinated $\text{trans-NiCl}_4\text{N}_2$, connected into infinite linear NiCl_2 chains with terminal bod ligands [ESI Section S2.3, Fig. S13-14, Table S5], though we also were also able to find crystals of $\text{NiCl}_2 \cdot 2\text{H}_2\text{O}$.¹⁸ Re-analysis of our PXRD data in the light of this new structure showed that it was primarily $\text{NiCl}_2(\text{bod})_2$ and a small quantity of nickel chloride hydrates. Further examination using single crystal electron diffraction of the remainder of the reaction mixture, which was dispersed as powder after being

dried and lightly ground onto a holey carbon grid, revealed that the sample contained a number of different phases with unit cells closely related to $\text{NiCl}_2(\text{btd})$, though with slightly different symmetries [ESI Section S2.4, Fig. S15-18, Table S6].¹⁶ Comparison of refinements with only bod, only btd and mixed ligand showed that the sample included nanocrystals of a monoclinic twinned $\text{NiCl}_2(\text{bod})$ and an orthorhombic polymorph of $\text{NiCl}_2(\text{btd})$, although we cannot exclude that this orthorhombic phase includes a low proportion of bod (<5%). We note these phases are not seen in the bulk PXRD and hence, we ascribe the formation of a small number of nanocrystals of $\text{NiCl}_2(\text{btd})$ to the presence of adventitious btd, likely facilitated by its high vapour pressure. This highlights the capability of electron diffraction to find and solve the structures of even minor crystalline phases.

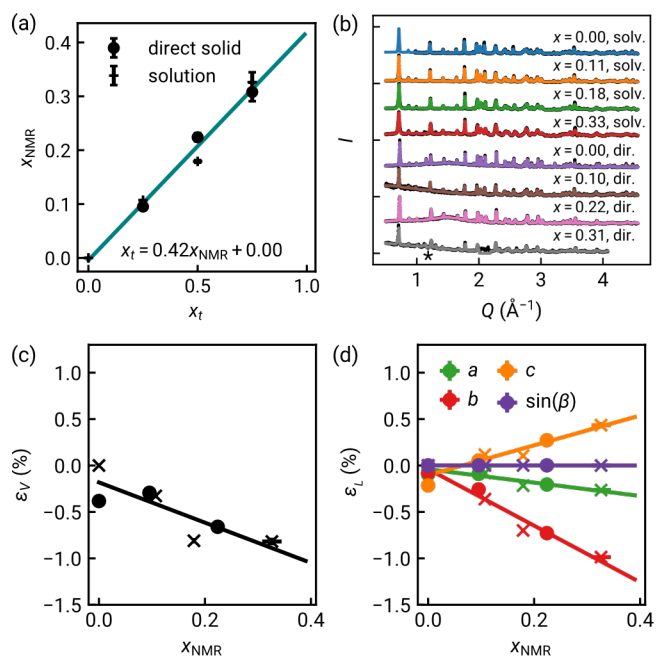


Fig. 2 Characterisation of mixed ligand $\text{NiCl}_2(\text{btd})_{1-x}(\text{bod})_x$ (a) Determination of x through integration of solution ^1H NMR spectra. Linear fit to data shown. (b) PXRD patterns for the solid-solution series. Pawley refined fit shown by coloured lines, data in black points. Variation in (c) volume strain (ϵ_V) and (d) lattice parameter strain (ϵ_L). Linear fit shown. Data point for $x_{\text{NMR}} = 0.31$ synthesised direct in solid state excluded due to presence of significant ($\text{NiCl}_2 \cdot 6\text{H}_2\text{O}$).

To determine the btd:bod ratio, and hence x , we dissolved a portion of each sample in d_6 -DMSO and carried out solution state ^1H NMR [Fig. 2 (a), Fig. S1]. This revealed that the bod content determined by NMR, x_{NMR} , was uniformly bod-poor compared to the target composition. This, together with the formation of $\text{NiCl}_2(\text{bod})_2$ in preference to $\text{NiCl}_2(\text{bod})$, suggests that the more electron deficient bod ligand does not coordinate as readily as the btd ligand. This is further borne out by the lack of reported metal complexes containing bod as a ligand in the CSD. We found that the $x_{\text{NMR}} = 0.31$ ($x_t = 0.75$) sample synthesised through direct reaction was poorly crystalline and contained significant impurities, so has not been further analysed. We thus focussed on samples with $x_t \leq 0.75$ for solution state reaction and $x_t \leq 0.50$ for solid state samples.

Comparison of the Pawley derived unit cell volume and lattice parameters with the composition determined from NMR shows linear, Vegard's law-type behaviour. We find that the interlayer spacing, c , expands on incorporation of bod, with the M-L-M distance, b , in turn shortening. The contraction along b can be explained by the shorter N-N distance in bod than btd, which would predict $b_{\text{btd}} - b_{\text{bod}} = 0.40 \text{ \AA}$, which is in quantitative agreement with the fitted value of $0.391(7) \text{ \AA}$.^{19,20} The significant interlayer expansion cannot be easily rationalised by differences in the size between btd and bod, but seem rather to reflect subtle differences in the angle between N-Ni-N axes of neighbouring Ni octahedra, though may also suggest that the interlayer vdW forces are weaker for bod than btd. The relative lack of change along the a axis suggests that the NiCl_2 chain is relatively unperturbed by the differences in Ni-N bonding and that changes in intermolecular forces between bod and btd are not a driving factor. We find no evidence of superlattice reflections indicative of long-range ordering of the bod and btd ligands, and no clear evidence of structured diffuse scattering that would be a signature of local ordering, though this can be challenging to detect in powder diffraction measurements of 2D compounds.²¹ Having developed this solid-solution series, we then investigated their physical properties, focussing on the mechanical compressibility and magnetic properties.

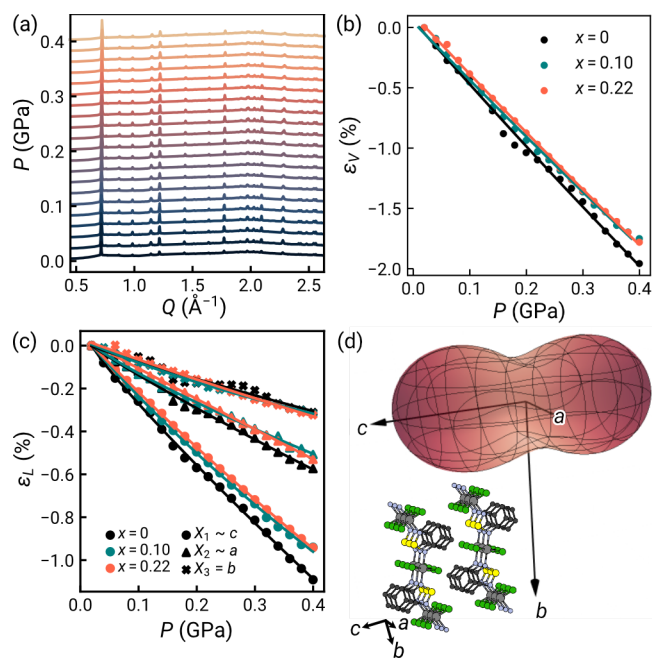


Fig. 3 High pressure synchrotron X-ray diffraction studies of $\text{NiCl}_2(\text{btd})_{1-x}\text{bod}_x$. (a) Stack plot showing evolution of patterns with pressure for $x = 0.22$. (b) Volumetric strain (ϵ_V) function of pressure, with second order Birch-Murnaghan fit shown.²² (c) Linear strain (ϵ_L) along each principal axis shown, with compressibility fit by an empirical equation of state,²³ (d) Linear compressibility indicatrix at $P = 0.2 \text{ GPa}$ for $x = 0.22$ shown, with crystal structure fragment shown in similar orientation.

We measured the compressibility of these materials using high pressure synchrotron X-ray powder diffraction at the I15 beamline of Diamond light source, using a hydraulic pressure cell to

obtain the fine pressure resolution required [Fig. 3].²⁴ This cell allows measurements from ambient to 0.4 GPa with pressure increments of $\Delta P = 0.02 \text{ GPa}$. We used silicone oil AP-100 as a pressure transmitting medium²⁵, which should be hydrostatic and non-penetrating in this pressure regime. We investigated here the doped samples synthesised directly using solid-state synthesis because they were more crystalline. The lattice parameters were refined using Pawley refinement. A limited number of impurity peaks were identified and fitted using additional structure free peaks [ESI Section S2.2, Figs. S4-12, Tables S2-4].

We found no evidence of pressure-induced framework degradation or phase transitions up to 0.4 GPa . Fitting of the pressure dependence of the volume using the second-order Birch-Murnaghan equation of state²² was carried out using the PASCAL Python package²⁶, and revealed that the bulk compressibility was $B_0 = 18.7(3) \text{ GPa}$ for the pure $\text{NiCl}_2(\text{btd})$, with the two doped samples both slightly stiffer: $x = 0.10$ has $B_0 = 20.6(0.3) \text{ GPa}$ and $x = 0.22$ has $B_0 = 19.96(13) \text{ GPa}$ [Fig. 3(b)]. These values are comparable to those reported for other nickel(II) layered materials, e.g. $\text{Ni}(\text{NCS})_2$ $B_0 = 17.0(2) \text{ GPa}$,²⁷ and NiI_2 $B_0 = 27.7(9) \text{ GPa}$,²⁸ and stiffer than $\text{ZnCl}_2(3,5\text{-dichloropyridine})_2$, $B_0 = 14.52(8)$, which contains 1D ZnCl_2 chains.²⁹

Our X-ray diffraction measurements allow us to determine not only the bulk modulus, but how the compressibility varies with direction. We find that the principal compressibilities do approximately coincide with the crystallographic axes, although in a monoclinic system the principal strains will not lie in general, along the unit cell axes. The compressibility is largest along the interlayer direction, X_1 ($\sim c$) $K_1 = 27.3(3) \text{ TPa}^{-1}$. X_2 ($\sim a$) is next stiffest, corresponding to the Ni-Cl-Ni chain direction, $K_2 = 14.8(4) \text{ TPa}^{-1}$, with the stiffest direction being the X_3 (b) along the Ni-N-(O/S)-N-Ni bonds direction, $K_3 = 7.7(4) \text{ TPa}^{-1}$ [Fig. 3(c,d), ESI Table S1]. The softness of X_1 is typical of vdW layered materials, e.g. $\text{Ni}(\text{NCS})_2$ $K_{\text{vdW}} = 32.5(2) \text{ TPa}^{-1}$, where K_{vdW} is the compressibility normal to the vdW layers. As inorganic materials tend to be less compressible, the direction with purely inorganic connectivity might be expected to be the stiffest, but in fact it is nearly twice as soft as the direction with purely metal-organic connectivity. This perhaps is due to the fact that the X_3 direction primarily involves direct bond compression, whereas the X_2 direction corresponds to bending of the Ni-Cl-Ni angle, although it is notable that DFT calculations suggest significant $\pi - \pi$ -interactions between the organic ligands along this direction which may modulate the compressibility.¹⁶ This trend is consistent with previous investigations of metal organic materials, such as in $[\text{CuCl}(\text{pyrazine})_2]\text{BF}_4$ where the Cu-pyrazine-Cu plane was significantly stiffer than the Cu-Cl-Cu chains,³⁰ and the plastically deforming $\text{ZnCl}_2(3,5\text{-dichloropyridine})_2$, where the ZnCl_2 chains are as soft as the vdW directions ($K_{\text{ZnCl}_2} \approx 23 \text{ TPa}^{-1}$).

As the structure is anisotropic, doping with bod also changes the compressibility differently in different directions. The interlayer direction becomes notably stiffer, with compressibility dropping to $24.7(4) \text{ TPa}^{-1}$ ($x = 0.10$) and $24.70(11) \text{ TPa}^{-1}$ ($x = 0.20$). Within the plane, the inorganic X_2 axis becomes slightly stiffer, $12.6(2) \text{ TPa}^{-1}$ ($x = 0.10$) and $14.1(3) \text{ TPa}^{-1}$ ($x = 0.20$), whereas

the organic X_3 axis in fact softens, $8.14(16)$ TPa $^{-1}$ ($x = 0.10$) and $8.9(4)$ TPa $^{-1}$ ($x = 0.20$) [ESI Table S1]. This suggests that organic substitution can be used to subtly modify the compressibility of MOMs, as found for MOFs,³¹ and hence the efficacy of strain tuning, whether in bulk or on surface.^{32,33}

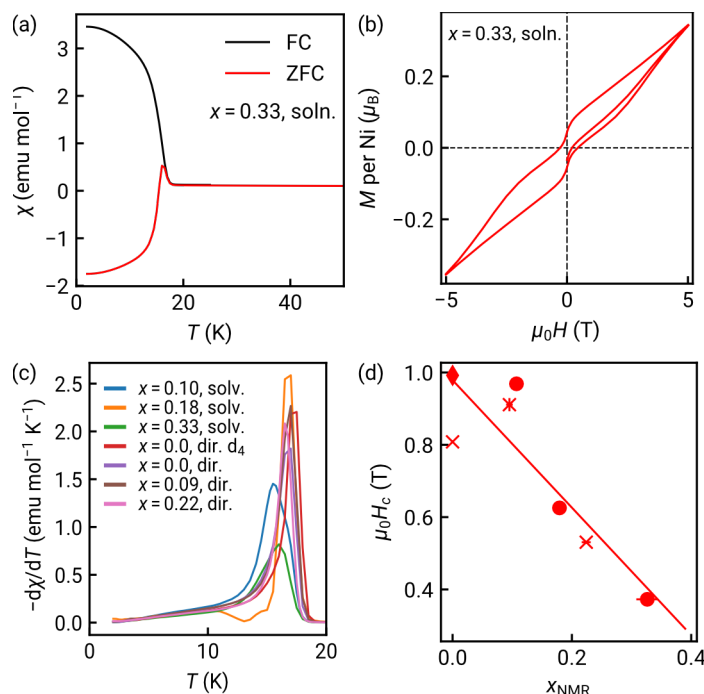


Fig. 4 Magnetic characterisation of the most heavily doped sample ($x = 0.33$, solution), showing (a) susceptibility $\chi(T)$ for samples cooled in magnetic field (FC) and in zero field (ZFC) and (b) isothermal magnetisation, $M(H)$, at $T = 2$ K. The variation in magnetic properties with x , (c) ordering temperature T_C with x , shown by the peak in $\frac{d\chi}{dT}$ and (d) variation in coercive field H_c . Linear fit to data shown.

We also investigated the magnetic properties of these MOMs, looking at all five solid-solution samples, plus the pure NiCl $_2$ (btd) (i.e. $x = 0$) and comparing to the deuterated sample previously reported NiCl $_2$ (btd-d $_4$) [Fig. 4, ESI Section S3, Figs. S19-22, Table S7].¹⁶ All the samples are canted (weak) ferromagnets, with a ferromagnetic ordering temperature $T_C = 17(1)$ K, and substantial magnetic hysteresis [Fig. 4(a,b,d), ESI Fig. S33, Table S7]. Doping does not greatly affect the ordering temperature, despite the substitution of S for O occurring along the superexchange pathway [Fig. 4(c), ESI Fig. S20, Table S7]. By contrast, the field dependence of the magnetism systematically varies on doping with bod, with the more bod added the softer the magnet [Fig. 4(d), ESI Table S7]. The drop in hysteresis can be seen most clearly in the coercive field, H_c , which decreases by 60% on doping with 33% bod (i.e. $x = 0.33$). The reduction in hysteresis suggests that the O atom has weaker spin-orbit coupling and is more electronegative, reducing the ligand field, which will together reduce the single-ion anisotropy. It is also possible that the slight differences in tilt angles between NiCl $_2$ chains induced by the differences in internal bond angles between bod and btd change the degree of canting, though this is not clearly observed, and the

changes in H_c are much larger than predicted by geometry alone.

The effect of isovalent substitution on magnetic function we observe is consistent with previous studies: replacing S with Se in NiPS $_3$ and Co(NCS) $_2$ (pyridine) $_2$ does not produce large changes in the ordering temperature, with a reduction in T_c of 5% in NiPS $_3$,³⁴ and an increase in T_c of 30% (1.5 K) for Co(NCS) $_2$ (pyridine) $_2$;³⁵ but this change does completely switch the single ion anisotropy from easy-plane anisotropy in NiPS $_3$ to easy-axis anisotropy for NiPSe $_3$.³⁴ The large effects on magnetic properties we observe is in contrast to the layered ZIF analogues where the organic substituents on the imidazolates had relatively small effects on both ordering temperature and fitted superexchange parameters,^{10,36} suggesting that substitution of atoms more directly on the superexchange pathway is critical to produce large effects. Previous work has shown that pressure can tune noncollinearity in MOMs,³⁷ and so the combination of mechanical and magnetic tunability we demonstrate suggests that doping will be an effective method to modulate strain switchability.

In conclusion, we report two methods for the synthesis of solid-solutions of NiCl $_2$ (btd) $_{1-x}$ (bod) $_x$. We find that there is an approximately linear dependence of the lattice parameters on ligand substitution, with the expected contraction along the M-L-M chain on doping with the smaller bod ligand. The btd ligand is preferentially incorporated into the structure, likely as it is a more electron rich ligand. Investigation of the mechanical properties using high pressure synchrotron X-ray diffraction showed that incorporation of bod stiffens the framework, primarily due to a reduction in interlayer compressibility, as the layers themselves become slightly more compressible. The canted ferromagnetism is retained on doping but doping tunes the hysteresis, producing a significant reduction (up to 60%) in coercive field. These results demonstrate that functionalisation of organic ligands can be a valuable way to tune both the magnetic function and pressure-responsiveness of van der Waals metal-organic magnets.

Conflicts of interest

There are no conflicts to declare

Acknowledgements

M.J.C. and J.P. were supported by UKRI (EP/X042782/1). We acknowledge Diamond Light Source (UK) for beamtime on beamline I15 under proposal number CY30815-2. G. K. acknowledges support from the Heisenberg program (524525093). The authors thank EPSRC for funding (EP/X014606/1) and the National Electron Diffraction Facility for providing access. J.P.T. thanks Oleg Dolomanov and Horst Puschmann for advice and training in the use of Olex2 N-beam. Benjamin Weare is thanked for assistance with electron diffraction measurements.

Author Contributions

E.M., S.L. and J.P. synthesised the samples. E.M., J.P., S.M.K., S.H., G.K. and D.D. carried out the high pressure X-ray measurements. E.M., J.P. and M.J.C. carried out the bulk magnetic measurements. E.M. and S.L. carried out the laboratory PXRD and NMR measurements. E.M., S.L. and M.J.C. analysed the NMR

data and powder X-ray diffraction data. E.M. and M.J.C. analysed the bulk magnetic data. E.M., S.L. and S.P.A. measured and analysed the single crystal X-ray diffraction data. J.P.T. measured the electron diffraction data, J.P.T. and M.J.C. analysed the electron diffraction data. M.J.C. wrote the paper with input from all other authors.

Notes and references

- 1 M. Eddaoudi, J. Kim, N. Rosi, D. Vodak, J. Wachter, M. O'Keeffe and O. M. Yaghi, *Science*, 2002, **295**, 469–472.
- 2 X. Kong, H. Deng, F. Yan, J. Kim, J. A. Swisher, B. Smit, O. M. Yaghi and J. A. Reimer, *Science*, 2013, **341**, 882–885.
- 3 A. D. Burrows, L. C. Fisher, C. Richardson and S. P. Rigby, *Chem. Commun.*, 2011, **47**, 3380–3382.
- 4 S. Horike, Y. Inubushi, T. Hori, T. Fukushima and S. Kitagawa, *Chem. Sci.*, 2012, **3**, 116–120.
- 5 C.-C. Cao, C.-X. Chen, Z.-W. Wei, Q.-F. Qiu, N.-X. Zhu, Y.-Y. Xiong, J.-J. Jiang, D. Wang and C.-Y. Su, *J. Am. Chem. Soc.*, 2019.
- 6 P. Vervoorts, J. Stebani, A. S. J. Méndez and G. Kieslich, *ACS Materials Lett.*, 2021, **3**, 1635–1651.
- 7 A. E. Thorarindottir and T. D. Harris, *Chem. Rev.*, 2020, **120**, 8716–8789.
- 8 L. S. Xie, G. Skorupskii and M. Dincă, *Chem. Rev.*, 2020, **120**, 8536–8580.
- 9 A. Helal, Z. H. Yamani, K. E. Cordova and O. M. Yaghi, *National Science Review*, 2017, **4**, 296–298.
- 10 J. Lopez-Cabrelles, E. Miguel-Casañ, M. Esteve-Rochina, E. Andres-Garcia, I. Vitorica-Yrzebal, J. Calbo and G. M. Espallargas, *Chem. Sci.*, 2022, **13**, 842–847.
- 11 J. Song, R. Pallach, L. Frentzel-Beyme, P. Kolodzeiski, G. Kieslich, P. Vervoorts, C. L. Hobday and S. Henke, *Angew. Chem. Int. Ed.*, 2022, **61**, e202117565.
- 12 T. Li, S. Jiang, N. Sivasdas, Z. Wang, Y. Xu, D. Weber, J. E. Goldberger, K. Watanabe, T. Taniguchi, C. J. Fennie, K. F. Mak and J. Shan, *Nat. Mater.*, 2019, 1–6.
- 13 F. Aribot, L. Voigt, M. A. Dunstan, W. Wan, J. N. McPherson, M. Kubus, N. J. Yutronkie, C. J. McMonagle, M. Coletta, A. S. Manvell, A. Viborg, S. Wong, K. A. Stampe, V. Baran, A. Senyshyn, M. D. Le, H. C. Walker, A. Chanda, F. Trier, N. Pryds, F. Wilhelm, M. R. Probert, N. B. Christensen, E. K. Brechin, A. Rogalev and K. S. Pedersen, *Molecular Alloying Drives Valence Change in a van Der Waals Antiferromagnet*, 2024.
- 14 S. Mondal, M. Kannan, M. Das, L. Govindaraj, R. Singha, B. Satpati, S. Arumugam and P. Mandal, *Phys. Rev. B*, 2019, **99**, 180407.
- 15 C. A. Occhialini, L. G. P. Martins, Q. Song, J. S. Smith, J. Kapeghian, D. Amoroso, J. J. Sanchez, P. Barone, B. Dupé, M. J. Verstraete, J. Kong, A. S. Botana and R. Comin, 2023.
- 16 J. Pitcairn, M. A. Ongkiko, A. Iliceto, P. Speakman, S. Calder, M. Cochran, J. Padison, C. Liu, S. Argent, A. Morris and M. Cliffe, *J. Am. Chem. Soc.*, 2024, **146**, 19146–19159.
- 17 G. S. Papaefstathiou, S. P. Perlepes, A. Escuer, R. Vicente, A. Gantis, C. P. Raptopoulou, A. Tsohos, V. Psycharis, A. Terzis and E. G. Bakalbassis, *J. Solid State Chem.*, 2001, **159**, 371–378.
- 18 B. Morosin, *Acta Cryst.*, 1967, **23**, 630–634.
- 19 T. Suzuki, T. Tsuji, T. Okubo, A. Okada, Y. Obana, T. Fukushima, T. Miyashi and Y. Yamashita, *J. Org. Chem.*, 2001, **66**, 8954–8960.
- 20 M. R. Ams, N. Trapp, A. Schwab, J. V. Milić and F. Diederich, *Chem. – Eur. J.*, 2019, **25**, 323–333.
- 21 M. L. Robinson, E. Whitaker, L. Jin, M. A. Hayward and G. Laurita, *Inorg. Chem.*, 2020, **59**, 3026–3033.
- 22 F. Birch, *Phys. Rev.*, 1947, **71**, 809–824.
- 23 A. L. Goodwin, D. A. Keen and M. G. Tucker, *Proc. Natl. Acad. Sci. U. S. A.*, 2008, **105**, 18708–18713.
- 24 N. J. Brooks, B. L. L. E. Gauthe, N. J. Terrill, S. E. Rogers, R. H. Templer, O. Ces and J. M. Seddon, *Rev. Sci. Instrum.*, 2010, **81**, 064103.
- 25 S. Dissegna, P. Vervoorts, C. L. Hobday, T. Düren, D. Daisenberger, A. J. Smith, R. A. Fischer and G. Kieslich, *J. Am. Chem. Soc.*, 2018, **140**, 11581–11584.
- 26 M. Lertkiattrakul, M. L. Evans and M. J. Cliffe, *J. Open Source Softw.*, 2023, **8**, 5556.
- 27 M. Geers, D. M. Jarvis, C. Liu, S. S. Saxena, J. Pitcairn, E. Myatt, S. A. Hallweger, S. M. Kronawitter, G. Kieslich, S. Ling, A. B. Cairns, D. Daisenberger, O. Fabelo, L. Cañadillas-Delgado and M. J. Cliffe, *Phys. Rev. B*, 2023, **108**, 144439.
- 28 M. P. Pasternak, R. D. Taylor, A. Chen, C. Meade, L. M. Falicov, A. Giesekus, R. Jeanloz and P. Y. Yu, *Phys. Rev. Lett.*, 1990, **65**, 790–793.
- 29 X. Liu, A. A. L. Michalchuk, B. Bhattacharya, N. Yasuda, F. Emmerling and C. R. Pulham, *Nat Commun*, 2021, **12**, 3871.
- 30 R. Scatena, F. Montisci, A. Lanza, N. P. M. Casati and P. Macchi, *Inorg. Chem.*, 2020, **59**, 10091–10098.
- 31 L. R. Redfern, L. Robison, M. C. Wasson, S. Goswami, J. Lyu, T. Islamoglu, K. W. Chapman and O. K. Farha, *J. Am. Chem. Soc.*, 2019.
- 32 D. L. Esteras, A. Rybakov, A. M. Ruiz and J. J. Baldoví, *Nano Lett.*, 2022, **22**, 8771–8778.
- 33 J. Cenker, S. Sivakumar, K. Xie, A. Miller, P. Thijsen, Z. Liu, A. Dismukes, J. Fonseca, E. Anderson, X. Zhu, X. Roy, D. Xiao, J.-H. Chu, T. Cao and X. Xu, *Nat. Nanotechnol.*, 2022, **17**, 256–261.
- 34 R. Basnet, K. M. Kotur, M. Rybak, C. Stephenson, S. Bishop, C. Autieri, M. Birowska and J. Hu, *Phys. Rev. Res.*, 2022, **4**, 023256.
- 35 T. Neumann, M. Rams, Z. Tomkowicz, I. Jess and C. Näther, *Chem. Commun.*, 2019, **55**, 2652–2655.
- 36 J. López-Cabrelles, S. Mañas-Valero, I. J. Vitorica-Yrezabal, M. Šiškins, M. Lee, P. G. Steeneken, H. S. J. van der Zant, G. Mínguez Espallargas and E. Coronado, *J. Am. Chem. Soc.*, 2021.
- 37 I. E. Collings, R. S. Manna, A. A. Tsirlin, M. Bykov, E. Bykova, M. Hanfland, P. Gegenwart, S. van Smaalen, L. Dubrovinsky and N. Dubrovinskaja, *Phys. Chem. Chem. Phys.*, 2018, **20**, 24465–24476.